


# Phase-dependent local brain states determine the impact of image-guided transcranial magnetic stimulation on motor network electroencephalographic synchronization

Davide Momi<sup>1,2</sup> , Recep A. Ozdemir<sup>1</sup>, Ehsan Tadayon<sup>1</sup>, Pierre Boucher<sup>1</sup>, Alberto Di Domenico<sup>3</sup>, Mirco Fasolo<sup>3</sup>, Mouhsin M. Shafi<sup>1,5</sup>, Alvaro Pascual-Leone<sup>4,5,6</sup> and Emiliano Santarnecchi<sup>1,7</sup>

<sup>1</sup>Berenson-Allen Center for Non-Invasive Brain Stimulation, Beth Israel Deaconess Medical Center, Boston, MA, USA

<sup>2</sup>Department of Neuroscience, Imaging and Clinical Sciences, University of Chieti-Pescara, Chieti, Italy

<sup>3</sup>Department of Psychological Science, Humanities and Territory, University of Chieti-Pescara, Chieti, Italy

<sup>4</sup>Hinda and Arthur Marcus Institute for Aging Research and Deanna and Sidney Wolk Center for Memory Health, Hebrew SeniorLife, Boston, MA, USA

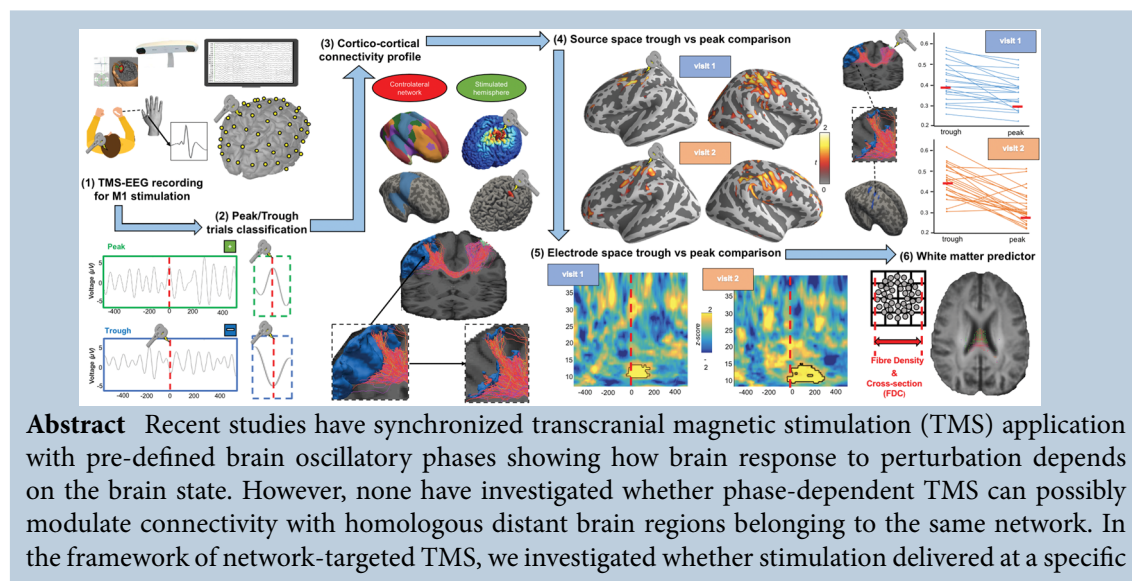
<sup>5</sup>Department of Neurology, Harvard Medical School, Boston, MA, USA

<sup>6</sup>Guttmann Brain Health Institute, Guttmann Institut, Universitat Autònoma, Barcelona, Spain

<sup>7</sup>Precision Neuroscience & Neuromodulation Program, Massachusetts General Hospital & Harvard Medical School, Boston, MA, USA

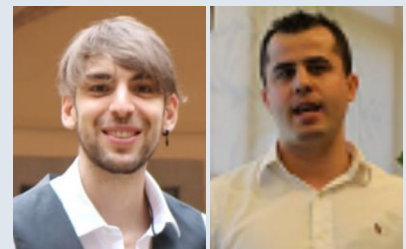
Edited by: Katalin Toth & Dario Farina

The peer review history is available in the Supporting Information section of this article (<https://doi.org/10.1113/JP282393#support-information-section>).



**Abstract** Recent studies have synchronized transcranial magnetic stimulation (TMS) application with pre-defined brain oscillatory phases showing how brain response to perturbation depends on the brain state. However, none have investigated whether phase-dependent TMS can possibly modulate connectivity with homologous distant brain regions belonging to the same network. In the framework of network-targeted TMS, we investigated whether stimulation delivered at a specific

**Davide Momi** completed his PhD at the Department of Neuroscience, Imaging and Clinical Sciences at the University G. d'Annunzio of Chieti. His project was focused on predicting the TMS signal propagation at the network-level, based on neuroimaging and electrophysiological data. He is currently a post-doctoral research fellow at CAMH (Toronto) where he is working on developing a computational model of TMS outcomes by combining neuroimaging and electrophysiological data. **Recep Ozdemir** completed his PhD at the University of Houston where he conducted studies investigating electrocortical biomarkers of human locomotion and postural control. After his PhD, he joined the University of Miami as a postdoctoral research fellow where he was involved in inducing plasticity protocols in patients with spinal cord injury. Afterwards, he joined the Berenson-Allen Centre for Noninvasive Brain Stimulation to study test-retest reliability of TEPs measures. He is currently an Instructor in Neurology at the Harvard Medical School.



phase of ongoing brain oscillations might favour stronger cortico-cortical (c-c) synchronization of distant network nodes connected to the stimulation target. Neuronavigated TMS pulses were delivered over the primary motor cortex (M1) during ongoing electroencephalography recording in 24 healthy individuals over two repeated sessions 1 month apart. Stimulation effects were analysed considering whether the TMS pulse was delivered at the time of a positive (peak) or negative (trough) phase of  $\mu$ -frequency oscillation, which determines c-c synchrony within homologous areas of the sensorimotor network. Diffusion weighted imaging was used to study c-c connectivity within the sensorimotor network and identify contralateral regions connected with the stimulation spot. Depending on when during the  $\mu$ -activity the TMS-pulse was applied (peak or trough), its impact on inter-hemispheric network synchrony varied significantly. Higher M1–M1 phase-lock synchronization after the TMS-pulse (0–200 ms) in the  $\mu$ -frequency band was found for trough compared to peak stimulation trials in both study visits. Phase-dependent TMS delivery might be crucial not only to amplify local effects but also to increase the magnitude and reliability of the response to the external perturbation, with implications for interventions aimed at engaging more distributed functional brain networks.

(Received 19 September 2021; accepted after revision 10 November 2021; first published online 20 November 2021)

**Corresponding author** E. Santarnecchi: Precision Neuroscience & Neuromodulation Program, Massachusetts General Hospital & Harvard Medical School, Boston, MA, USA. Email: esantarnecchi@mgh.harvard.edu

**Abstract figure legend** TMS pulses delivered over M1 at the negative peak of  $\mu$ -frequency band induces higher phase-lock synchronization with interconnected contralateral homologous regions. The fiber density and cross-section of the white matter tract that connect the two motor cortices predicts such cortico-cortical synchronization changes. Phase-dependent TMS delivery might be crucial to increase magnitude and reliability of within-network synchronization.

### Key points

- Synchronized transcranial magnetic stimulation (TMS) pulses with pre-defined brain oscillatory phases allow evaluation of the impact of brain states on TMS effects.
- TMS pulses over M1 at the negative peak of the  $\mu$ -frequency band induce higher phase-lock synchronization with interconnected contralateral homologous regions.
- Cortico-cortical synchronization changes are linearly predicted by the fibre density and cross-section of the white matter tract that connects the two brain regions.
- Phase-dependent TMS delivery might be crucial not only to amplify local effects but also to increase the magnitude and reliability of within-network synchronization.

## Introduction

In the last two decades transcranial magnetic stimulation (TMS) has been extensively tested for the treatment of several neurological and psychiatric disorders (Connolly *et al.* 2012). Even though TMS provides a safe and well tolerated therapeutic option for several neuro-psychiatric conditions, and several TMS devices have been cleared by the Food and Drug Administration and other regulatory bodies, findings often show high variability and sometimes small effect sizes reflecting only moderate clinical improvement (López-Alonso *et al.* 2014). It is well known that the impact of a TMS pulse on the neural system is not determined only by the properties of the stimulus but also by the initial brain

state of the perturbed region (Silvanto & Pascual-Leone, 2008). Brain states can be non-invasively measured by electroencephalography (EEG) and the underlying cortical activity can be characterized, for example, by ongoing oscillations (Buzsáki, 2006). Such oscillations represent a fundamental mechanism enabling brain network communication at multiple temporal and spatial scales which sustain both sensory processing and higher order coordination of motor and cognitive functions (Buzsáki & Draguhn, 2004; Uhlhaas & Singer, 2010; Akam & Kullmann, 2014). A compelling way to explore the neurophysiological significance of such oscillations is to combine TMS and EEG (Thut & Pascual-Leone, 2010; Voineskos *et al.* 2010). Indeed, the effects of controlled and well-timed perturbations induced by TMS pulses can

be measured by EEG, which assesses both local induction of brain activity and its millisecond-level propagation throughout the brain (Momi *et al.* 2020). It is also possible to study the impact of specific brain states at the time of stimulation on the TMS-induced effects (Bergmann *et al.* 2019; Schaworonkow *et al.* 2019) and relate those to cognitive or behavioural consequences. For this reason, in the last years multiple efforts have been made to individualize the treatment of several disorders taking into account, for example, spontaneous brain oscillation (Drysdale *et al.* 2017) and neural excitability (Perera *et al.* 2016), in order to investigate the contribution of these components to the variability in the TMS interventions. In this context, recent studies have started to deliver individual or trains of external pulses during pre-defined brain oscillatory phases, reporting promising results within the motor system in healthy individuals (Stefanou *et al.* 2018) and stroke patients (Hussain *et al.* 2020). Specifically, phase-dependent TMS applied during the negative peak (trough) of the sensorimotor  $\mu$ -frequency band (8–13 Hz) increased corticospinal behavioural output (Zrenner *et al.* 2018) and brain TMS evoked-potentials (TEPs) (Desideri *et al.* 2019) to a larger extent than TMS applied irrespective of this phase. Such results are based on the fact that the trough of the  $\mu$ -oscillation represents a state where the dendritic trees of pyramidal neurons are closer to the firing threshold and, therefore, more likely to generate action potentials in response to a TMS pulse (Buzsáki *et al.* 2012). However, it is worth mentioning that another research group did not find any consistent modulatory effect of  $\mu$ -phase on corticospinal excitability using brain state-informed TMS targeting the peak and trough (Madsen *et al.* 2019). Such a discrepancy in the findings of the two groups might be due to several differences in the experimental approach such as the number of trials per condition, the inter-stimulus interval (ISI) between the TMS pulses and the statistical model employed for the analyses.

Despite the aforementioned studies having evaluated the behavioural and brain evoked-potential outcomes following phase-dependent TMS application, none so far have investigated possible changes in cortico-cortical (c-c) synchronization of homologous brain regions belonging to the same network. In this study we used image-guided TMS-EEG to selectively perturb the primary motor cortex (M1) and further investigate whether c-c connectivity is modulated by the phase of the ongoing sensorimotor  $\mu$ -rhythm. Given that the aforementioned studies have demonstrated how the trough of the  $\mu$ -rhythm represents a high-excitability state (Zrenner *et al.* 2018; Desideri *et al.* 2019), we hypothesized that external perturbation at the negative peak would be able to induce higher c-c synchrony between the stimulated target region and homologous regions of the same network compared to stimulation over the peak. It is important to mention that

that the focus of our analysis was on the contralateral homologous motor regions connected to the stimulated spot via transcallosal white matter fibres in accordance with recent publications (Zrenner *et al.* 2018; Desideri *et al.* 2019; Bortoletto *et al.* 2021; Zazio *et al.* 2021). In order to identify the individual sensorimotor network, Schaefer's atlas (Schaefer *et al.* 2018) was employed, which divided the brain into seven networks.

Finally, control analyses were conducted to investigate if microstructural properties of the white matter were related to c-c synchronization. Importantly, considering the quest for data reproducibility, the same analyses were repeated on data collected on the same sample of healthy individuals across two separate study visits 1 month apart.

## Methods

### Participants

The study was approved by the Institutional Review Board of the Beth Israel Deaconess Medical Center (2016P000351). Each participant was asked to provide written informed consent and was remunerated for the entire study; the study conformed to the *Declaration of Helsinki*. Twenty-four right-handed (Oldfield, 1971) healthy volunteers (mean age,  $32 \pm 10$  years; range, 19–49 years) with normal neurological and psychiatric evaluation and no history of drugs acting on the central nervous system were recruited through flyers and on-line advertisement. A pre-TMS magnetic resonance imaging (MRI) assessment was carried out including a T1-weighted (T1w) anatomical, a resting state fMRI and a diffusion-weighted imaging (DWI) scan. Such imaging assessment was carried out in order to extract individualized networks maps (Fig. 1A). Each participant subsequently carried out two TMS visits, separated by 1 month, where 120 single pulses (for each visit) were delivered every 5–8 s (random jitter) over M1 (Fig. 1B). The TMS spot was personalized based on individual resting motor threshold (RMT), defined as the lowest stimulation intensity necessary to evoke a motor evoked potential (MEP) ( $\sim 50 \mu\text{V}$ ) in at least 50% of the trials (Rossini *et al.* 2015). The 'hotspot' of stimulation was therefore determined as the cortical hand region where MEPs were larger and more consistent in the right first dorsal interosseous (FDI) muscle, as compared to abductor pollicis brevis (APB) muscle (Rothwell *et al.* 1999). During the stimulation application, participants were asked to wear earplugs (Rossi *et al.* 2020) where auditory white noise was played to minimize the impact of the TMS click (ter Braack *et al.* 2015). A thin layer of foam was placed under the TMS coil to minimize somato-sensory contamination of the TMS-evoked EEG potentials. The stimulation intensity was set at 120%

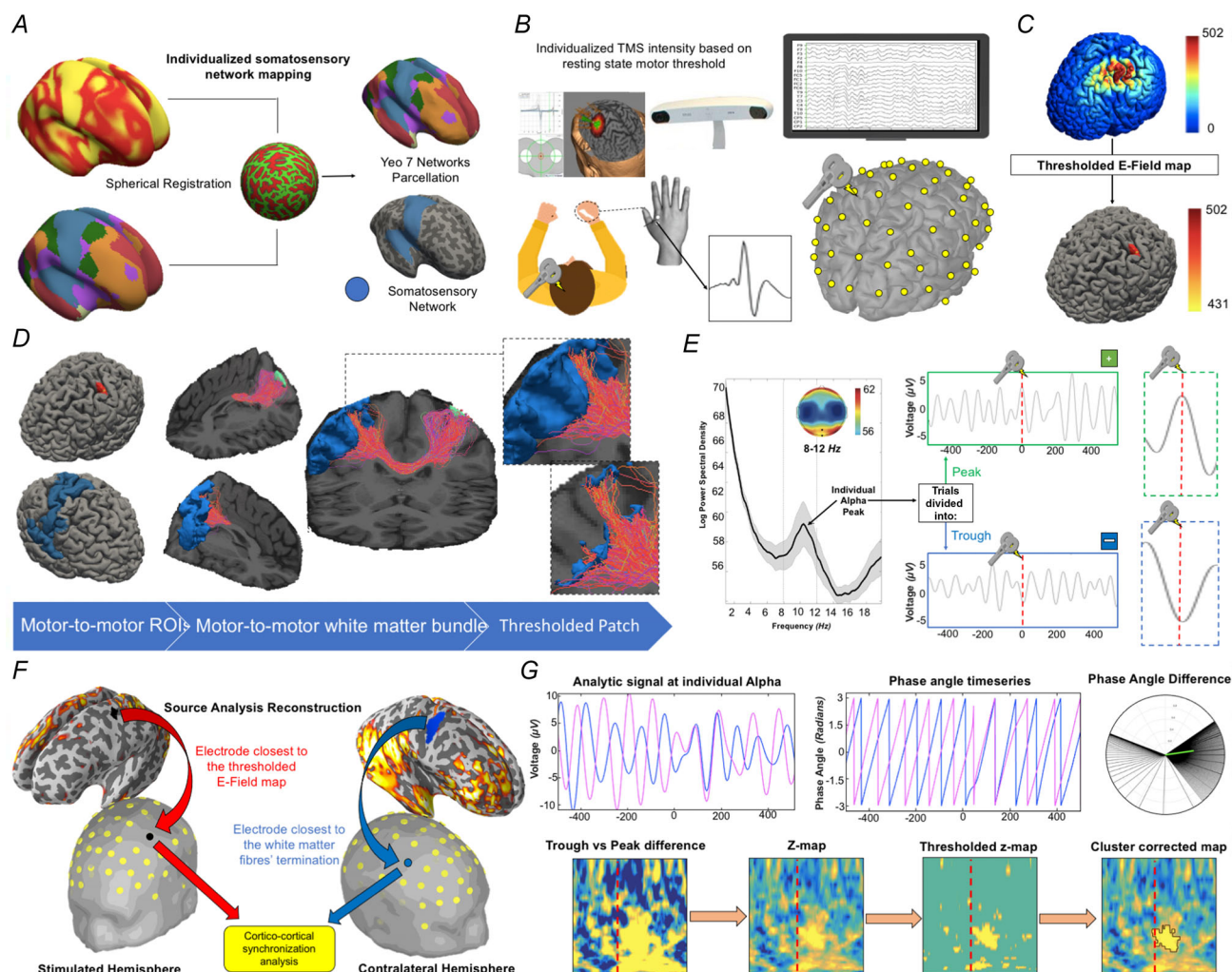


**Figure 1. Methodological workflow and metrics extraction**

A, in order to identify the contralateral motor network, the 7-network functional cortical atlas (Yeo *et al.* 2011) was projected onto the subject's cortical surface using the spherical registration implemented in Freesurfer software. B, TMS was applied to the individual left primary motor area (M1) 'hotspot' determined as the cortical hand region where MEPs were larger and more consistent in the right first dorsal interosseus (FDI) muscle, as compared to abductor pollicis brevis (APB) muscle (Rothwell *et al.* 1999). Once the 'hotspot' was identified by evaluating MEPs responses, anatomical MRI was used for the neuronavigation of the TMS spot while high-density (hd)-EEG with 64 channels was simultaneously recorded. C, TMS-induced electric field was modelled with SimNIBS (Thielscher *et al.* 2015). The point with maximal electric field (E-field) was then defined and from there a sphere of radius 0.5 cm was created. D, seed-based anatomically constrained tractography (Smith *et al.* 2012) was performed in order to extrapolate the white matter bundle connecting the E-field map and the contralateral sensorimotor network. The individual sensorimotor network map was thresholded using the reconstructed tract where only the vertices reached by a streamline were selected. The remaining vertices represent the cortical regions structurally connected with the stimulation spot. E, the time series from the electrode closest to the stimulation spot were extracted and filtered using the individual peak  $\mu$ -frequency (Corcoran *et al.* 2018). Then, trials were classified as peak or trough depending on whether the TMS pulse was delivered at the positive or the negative peak, respectively. In order to investigate how much the results would have depended on how close the TMS pulse was to the actual peak of the phase, TMS stimuli were classified as landing on a peak or trough using several sensitivity windows ranging from 5 ms (very accurate) to 40 ms (more liberal). TMS pulses that did not land within a given sensitivity window were not included in that analysis (see Methods for further details). F, as for the connectivity analysis at source level, metrics were extracted from the white matter fibres' terminations of the tract connecting the stimulated grey matter portion. As for electrode level analysis, the Euclidian distance was computed from every electrode and the centroid of the thresholded E-field map (stimulated hemisphere) and the white matter fibres' terminations (contralateral hemisphere). The closest electrodes for the left and right hemisphere were then selected for the TMS-EEG connectivity analysis. G, phase locking value (PLV) (Lachaux *et al.* 1999; Mormann *et al.* 2000) was calculated as a measure of connectivity for both source and electrode level analyses. The raw difference

between the PLV of trough and peak trials was calculated for all the frequencies between 3 and 40 Hz. Then, 1000 permutation *t*-tests were performed in which the surrogated trough vs. peak difference was computed after each iteration and statistically compared with the real difference (Pernet *et al.* 2015). Finally, the cluster threshold was determined as the 95th percentile of the cluster's surrogate distribution. [Colour figure can be viewed at [wileyonlinelibrary.com](http://wileyonlinelibrary.com)]

of the RMT with randomly jittered (5000–8000 ms) inter-stimulus intervals.

### Modelled and image-guided selection of electrodes

In order to perform c-c connectivity analysis, the portions of grey matter mainly affected by the TMS pulses were selected based on electric field (E-field) modelling (left hemisphere) and tractography (right hemisphere). TMS-induced E-field was modelled with SimNIBS (Thielscher *et al.* 2015) to identify the cortical region directly engaged by the external perturbation (Fig. 1C). Given that in the literature there is no consensus on how to selectively identify only the neural tissue recruited by the TMS pulse (Romero *et al.* 2019), we defined this as the point with the maximal E-field and from there created a sphere of radius 0.5 cm and used this as seed for connectivity analysis in source space. As for electrode level analysis, the Euclidian distance was computed from every electrodes of the stimulated hemisphere and the closest electrode to the thresholded E-field map was picked for connectivity analysis. Following this, in order to identify the contralateral motor network, the seven-network functional cortical atlas (Yeo *et al.* 2011) was projected onto the subject's cortical surface using the spherical registration implemented in Freesurfer software (Fig. 1A). The resulting maps were then resampled to native structural T1w MRIs. Seed-based anatomically constrained tractography (Smith *et al.* 2012) was performed in order to extrapolate the white matter bundle connecting the E-field map and the contralateral sensorimotor network (Fig. 1D). The reconstructed tract was used to threshold the sensorimotor network map where only the vertices reached by a streamline were selected. The remaining vertices represent the cortical regions structurally connected with the stimulation spot and were used to extract connectivity metrics in source space. As for electrode level analysis, the Euclidian distances between the largest area of the white matter fibres' termination cluster and the electrodes of the right hemisphere were computed and the closest electrode was picked. For further details on TMS-induced electric field modelling, see Supporting information.

### EEG trial partitioning in peak and trough

Based on previous studies which reported higher cortico-spinal excitability when the TMS pulse was delivered at

the negative peak of sensorimotor  $\mu$ -oscillation (Zrenner *et al.* 2018; Desideri *et al.* 2019), we first identified the individual sensorimotor rhythm (Fig. 1E). To this purpose, individual peak alpha frequency (PAF) and centre of gravity (CoG) were calculated from resting-state power spectra, which had been previously smoothed using a Savitzky–Golay filter (Corcoran *et al.* 2018).

A surface Laplacian spatial band-pass filter was then applied to the preprocessed EEG in order to control for volume conduction effects, attenuating activity from distant sources or activity that is highly spatially distributed and temporally coherent (Tenke & Kayser, 2012). The time series from the electrode closest to the stimulation spot (see dedicated section for details on electrode selection) were extracted and filtered using the individual PAF (filter width of  $\pm 2$  Hz). Thus, trials were classified as peak or trough depending on whether the TMS pulse was delivered at the positive or the negative peak respectively.

In order to evaluate the specificity of the phase-dependent TMS effects, different window sizes ranging from 5 ms (very accurate) to 40 ms (more liberal) were used during the classification of the trials into peak or trough. Specifically, pulses were classified as landing on a peak or trough if they fell within the sensitivity window (i.e.  $\pm 5$  ms) of the peak or trough of the ongoing oscillation. For instance, if the employed window size was 5 ms, the trials were classified as peak (or trough) if and only if the pulse was delivered  $\pm 5$  ms near the positive (or negative) phase peak. On the other hand, if the pulse of a given trial was delivered  $> 5$  ms distant from the peak, that trial was discarded and not included in subsequent analyses. Such differentiation was performed in order to evaluate how much the results depend on how close the TMS pulse was to the actual peak of the phase. Importantly the peak/trough ratio was included in all the statistical analyses as a covariate of nuisance.

### EEG source reconstruction and metrics

All TMS evoked EEG source reconstruction was performed in Minimum-Norm Estimate (MNE) software (Gramfort *et al.* 2013) (<https://mne.tools/stable/index.html>) running in Python 3.6 (Fig. 1F). First, the watershed algorithm was used to generate the inner skull, the outer skull and the outer skin surfaces triangulations. Then the EEG forward solution was calculated using a three compartment boundary-element model (Gramfort *et al.* 2010). Noise covariance was estimated from individual

trials using the pre TMS (−500 ms to 0 ms) time window as baseline. The inverse model solution of the cortical sources was performed using the dynamic statistical parametric mapping (dSPM) method with current density (Hämäläinen & Ilmoniemi, 1994) and constraining source dipoles to the cortical surface. The resulting output of EEG source reconstruction was the dSPM current density time series for each cortical vertex. In order to investigate inter-hemisphere c-c synchronization differences between trough and peak trial, whole-brain phase locking value (PLV) was computed from the thresholded individual E-field map for different frequencies (ranging from 3 to 40 Hz). Specifically, PLV was calculated as the length of the average of phase angle differences between electrodes over time (Lachaux *et al.* 1999; Mormann *et al.* 2000), resulting from the convolution between a complex Morlet wavelet and the data.

$$PLV_f = \left| n^{-1} \sum_{t=1}^n e^{i(\varphi_{b,t} - \varphi_{a,t})} \right|$$

where  $n$  is the number of time points and  $\varphi_b$  and  $\varphi_a$  are phase angles from electrodes  $b$  and  $a$  at frequency  $f$  for each time point  $t$ . By subtracting these phase angle vectors and computing their average length, the result will be between 0 for absent coupling and 1 for perfect synchrony.

The final PLV maps for trough and peak trial were then corrected for the baseline using the decibel conversion (Cohen, 2017) in order to account for both limitations of raw values and electrode-specific idiosyncratic characteristics.

$$dB_{t,f} = 10 \log_{10} \left( \frac{\overline{\text{activity}_{t,f}}}{\overline{\text{baseline}_f}} \right)$$

where the horizontal bar over baseline indicates the mean across the baseline time period, and  $t$  and  $f$  are time and frequency, respectively. Finally, individual PLV maps were morphed to average brain for group analysis where both permutation testing and cluster correction were implemented in order to compare trough *vs.* peak trials.

### EEG phase-based connectivity analysis

In order to investigate whether the connectivity results found at the source level were replicable also at the electrode level (Fig. 1G), PLV was also computed between the electrodes affected by the TMS pulse (see dedicated section for details on the electrode selection).

The baseline corrected time–frequency matrices for peak and trough were statistically compared using both a condition-wise permutation testing and a cluster-based thresholding (Pernet *et al.* 2015) as a correction for multiple comparisons. Specifically, the permutation test transformed the difference between the trough and the

peak trials into a  $z$ -value with respect to a null distribution of surrogate conditions difference values, obtained by swapping condition labels at each of 1000 permutations. The resulting  $z$ -scores were thresholded at  $P < 0.05$ . With an additional 1000 iterations permutation test, a distribution of cluster sizes of contiguous significant points under the null hypothesis of no difference was computed, and only the time–frequency clusters that exceeded the 95th percentile of this distribution was retained.

### DWI metrics computation

White matter fibre orientation distributions (FODs) were computed using MRtrix3Tissue (<https://3tissue.github.io/>) for each participant by ‘single-shell 3-tissue constrained spherical deconvolution’ (SS3T-CSD) (Dhollander & Connelly, 2016) using a group averaged response function for each tissue type (white matter (WM), grey matter (GM) and cerebrospinal fluid (CSF)) (Raffelt *et al.* 2012). Following these processing steps, we calculated the three standard fixel-based metrics for FBA (Raffelt *et al.* 2017):

- (1) Fibre density (FD): a microstructural metric that serves as a proxy for axonal density or packing.
- (2) Fibre cross-section (FC): a macrostructural metric that approximates relative fibre bundle diameter or size.
- (3) Fibre density and cross-section (FDC): the product of FD and FC, which encapsulates changes to both micro- and macro-structure.

### MRI data acquisition

The MRI evaluation was performed on a 3T scanner (GE Healthcare, Ltd, Hatfield, UK). The T1w was used for neuronavigation using theBrainsight™ TMS Frameless Navigation system (Rogue Research Inc., Montreal, Canada) as discussed below. The T1w was acquired using a 3D spoiled gradient echo sequence: 166 axial-oriented slices for whole-brain coverage; 240 mm isotropic field-of-view; 0.937 mm × 0.937 mm × 1 mm native resolution; flip angle = 15°; TE/TR ≥ 2.9/6.9 ms; duration ≥ 432 s. DWI sequences were collected using a single-shot echo planar imaging (slices = 71; matrix size = 256 × 256 × 71; voxel size = 0.8 mm × 0.8 mm × 2.2 mm; repetition time = 8500 ms, time echo = 79 ms; 30 non-colinear directions,  $b$ -value = 1000 s mm<sup>−2</sup>).

### DWI data preprocessing

A customized pipeline running in Ubuntu 18.04 LTS was used for the preprocessing of DWI images

using tools in FMRIB Software Library (FSL 5.0.3; [www.fmrib.ox.ac.uk/fsl](http://www.fmrib.ox.ac.uk/fsl)) (Jenkinson *et al.* 2012), Mrtrix3 ([mrtrix.readthedocs.io/en/latest/](http://mrtrix.readthedocs.io/en/latest/)) (Tournier *et al.* 2012), FreeSurfer (Fischl *et al.* 2004) and ANTs ([stnava.github.io/ANTs/](http://stnava.github.io/ANTs/)) (Avants *et al.* 2011). All images were denoised (Veraart *et al.* 2016), preprocessed via FSL's EDDY (Andersson & Sotiropoulos, 2016), and bias field corrected (Zhang *et al.* 2001). The response function for a single fibre population was estimated using a spherical deconvolution Tournier algorithm (Tournier *et al.* 2007). Simultaneously, the T1w images were coregistered to the  $b_0$  volume and then segmented using the FAST algorithm (Zhang *et al.* 2001). Two subjects were excluded from the analysis given poor quality in their DWI data.

## TMS

TMS was delivered using a figure-of-eight shaped coil with dynamic fluid cooling (Magspro 75mm cool B-65, Magpro A/S., Denmark) attached to a MagPro X-100 stimulator (MagVenture A/S, Denmark). T1w anatomical images were imported into the Brainsight™ TMS Frameless Navigation system (Rogue Research Inc.), and a coregistration procedure was performed using scalp landmarks (nasion, vertex and the two preauricular points) in order to monitor the coil position. MEPs were recorded with active electrodes positioned on the right FDI and the right APB muscles, while the reference electrode was placed over the metacarpophalangeal joint of the index finger. EMG data were amplified and digitized using a Powerlab 4/25T data acquisition system (ADInstruments, Colorado Springs, CO, USA) at a sampling rate of 4000 Hz (bandpass filtered at 10–2000 Hz). EMG signals were continuously streamed by using LabChart software (LabChart 8.0) to monitor MEPs, and epochs were recorded with a 150 ms window length covering from 50 before to 100 ms after the TMS pulse. The individual T1w was used to localize the anatomical cortical hand region before the TMS visit. This served as a starting point location for identifying the 'hotspot' which corresponded to the scalp location where TMS intensity was sufficient to evoke a motor response ( $\sim 50 \mu\text{V}$ ) in the FDI muscle in at least 50% of the trials.

## EEG

Whole scalp 64-channel EEG data were collected with a TMS-compatible amplifier system (actiCHamp system, Brain Products GmbH, Munich, Germany) and labelled in accordance with the extended 10–20 international system. EEG data were online referenced to the Fp1 electrode. Electrode impedances were maintained below  $5 \text{ k}\Omega$  at a sampling rate of 1000 Hz. EEG signals were digitized using a BrainCHamp DC amplifier and linked to Brain-

Vision Recorder software (version 1.21, Brain Products) for online monitoring. Digitized EEG electrode locations on the scalp are also co-registered to individual MRI scans using Brainsight™ TMS Frameless Navigation system.

## EEG data processing

A customized script running in MATLAB R2017b (The MathWorks Inc., Natick, MA, USA) was used for offline data preprocessing mainly performed with the EEGLAB 14.1 toolbox (Delorme & Makeig, 2004). A single block of 120 trials was first created by merging the two single blocks of 60 trials each, and then segmented into epochs of 1500 ms each (from  $-500$  (pre-pulse) to  $1000$  ms (post-pulse)). Baseline correction was performed using an amplitude of the mean pre-pulse ( $-500$  to  $-100$  ms) signal and raw data were visually inspected to then remove noisy channels. Zero-padding was applied on a window of  $-2$  to  $14$  ms to reject early TMS pulse artefact and noisy epochs were then removed based on the voltage ( $\geq 100 \mu\text{V}$ ), kurtosis ( $\geq 3$ ), joint probability (single channel-based threshold  $\geq 3.5$  SD) and visual inspection. In order to minimize overfitting and noise components, the dimensionality of the data was firstly reduced to 60 components by principal component analyses (PCA). Subsequently, a first round of fast independent component analysis (fICA) (Hyvärinen & Oja, 1997) was run specifically aimed at removing remaining early TMS-evoked and EMG artefacts. A linear interpolation was used to interpolate the zero-padded time window and the EEG data were then band pass filtered using a forward-backward fourth-order Butterworth filter from  $1$  to  $100$  Hz, notch filtered between  $57$  and  $63$  Hz, and referenced to global average. A second PCA was further employed to reduce the data dimensionality into 57 components before removing remaining artefact (e.g. eye movement/blink, muscle noise (EMG), single electrode noise, TMS evoked muscle, cardiac beats, auditory evoked potentials) with a second round of fICA (Rogasch *et al.* 2017). During both fICA, the components were visually inspected where a semi-automated artefact detection algorithm incorporated into the open source TMS-EEG Signal Analyser (TESA v0.1.0-beta; <https://nigelrogasch.github.io/TEESA>) was used (Rogasch *et al.* 2017). Finally, a low pass filtered with a fourth-order Butterworth filter at  $60$  Hz was employed, and previously removed channels were spherically interpolated.

## Control analyses

In order to test potential differences in the peak/trough ratio for visit 1 and visit 2, a  $2 \times 5$  ANOVA was run with the factor Visit (2 levels: visit 1 and visit 2) and Time (five levels: 40, 30, 20, 10 and 5 ms). No significant interaction

Visit  $\times$  Time ( $F_{(1,23)} = 0.55$ ,  $P = 0.46$ ) or main effect of Visit ( $F_{(1,23)} = 3.83$ ,  $P = 0.06$ ) and Time ( $F_{(1,23)} = 0.76$ ,  $P = 0.39$ ) were found.

Moreover, in order to control the specificity of the TMS-induced c-c phase-dependent connectivity for trough trials, 3 min of resting-state EEG collected during eyes open were analysed. Specifically, after data pre-processing, surrogate epochs were created with time windows compared to the TMS-evoked data. Afterwards, time series from the same electrode were extracted and filtered using the same individual peak  $\mu$ -frequency. Then, trials were categorized as peak or trough depending on whether the surrogate event occurred at the time of the positive or the negative peak, respectively. Topoplots cosine similarity was computed between resting-state and TMS-EEG data for both peak and trough trials.

Moreover, c-c connectivity of the resting-state period (from  $-500$  to  $0$  ms) preceding TMS was also extracted and compared to the post-TMS window for both peak and trough trials. To make this comparison, a  $2 \times 2 \times 4$  analysis of variance (ANOVA) was performed with a (within subjects) factor 'Trial' (two levels: Peak; Trough), a (within subjects) factor 'Time' (two levels: Pre-TMS; Post-TMS) as well as a (within subjects) factor 'Frequency' (four levels: Theta, Alpha, Beta, Gamma). The critical  $P$ -value was then adjusted using Bonferroni correction to account for multiple comparisons ( $*p < 0.05$  Bonferroni corrected). We hypothesized that TMS would induce

higher c-c synchrony between structurally connected brain regions compared to conventional resting-state EEG and specifically for trough trials.

## Results

### Source level phase-based connectivity between left and right hemisphere

In order to investigate c-c synchronization within the motor network, source-level individual PLV maps were computed using the thresholded E-field map as seed separately for trough and peak trials. As shown in Fig. 2A, a higher PLV value at an individual  $\mu$ -band was found with the contralateral somato-motor network for trough (visit 1: average PLV = 0.78; visit 2: average = 0.63) compared to peak (visit 1: average PLV = 0.33; visit 2: average = 0.21) trials. As shown in Fig. 2B, individual PLV scores extracted from thresholded streamline maps were significantly higher for trough compared to peak trials for both visit 1 ( $t = 4.58$ ,  $P < 0.001$ ) and visit 2 ( $t = 5.94$ ,  $P < 0.001$ ). Given that in the preprocessing steps the first 14 ms after the pulse were zero-padded, the connectivity analysis was re-run leaving out the first 15 ms after the pulse in order to control for this confounding factor. Results were substantially similar and are reported in Supplementary information, Results.

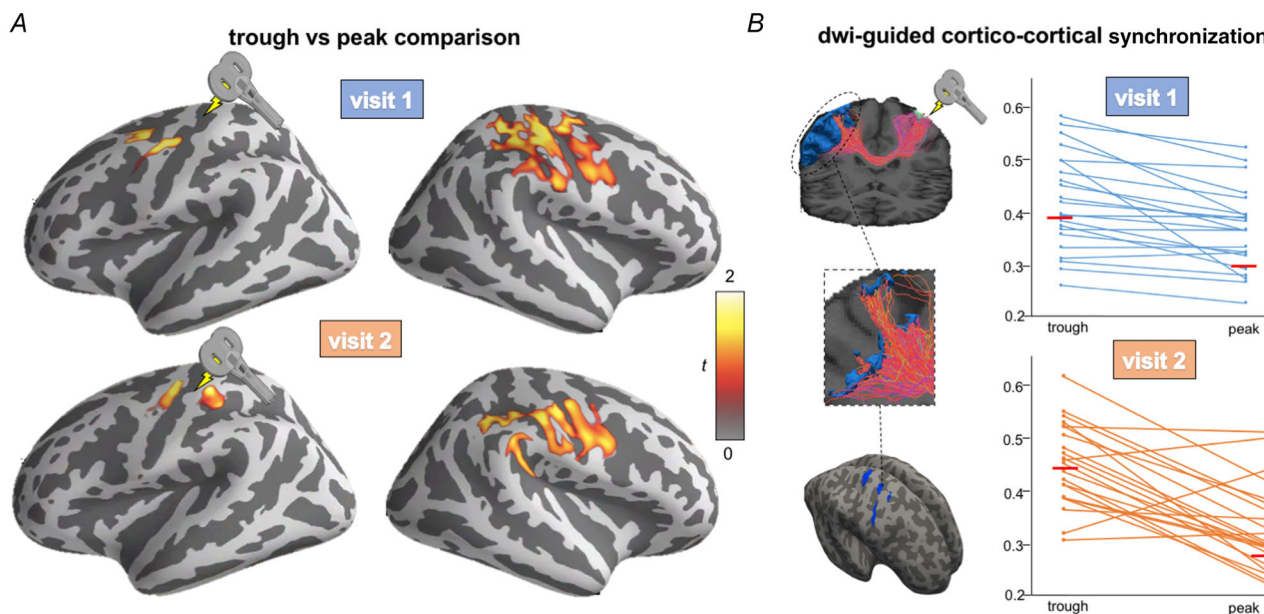


**Figure 2. Source level PLV whole-brain connectivity with the stimulated region**

A, significant cluster comparing PLV maps for trough vs. peak trials. Higher synchronization between the stimulated region and the contralateral hemisphere was found for both visit 1 (top) and visit 2 (bottom). B, individual PLV between the stimulated region and the thresholded streamline map. Higher synchronization was found for trough compared to peak trials for both visit 1 (top;  $t = 4.58$ ,  $P < 0.001$ ) and visit 2 (bottom;  $t = 5.94$ ,  $P < 0.001$ ). [Colour figure can be viewed at [wileyonlinelibrary.com](http://wileyonlinelibrary.com)]



### Electrodes selection and trough/peak ratio

Over the stimulated hemisphere (Fig. 3A, left), the electrodes closest to the centroid of the thresholded E-Field map were C3 (visit 1: 19/24; visit 2: 19/24), C1 (visit 1: 2/24; visit 2: 2/24), FC1 (visit 1: 1/24; visit 2: 0/24), FC3 (visit 1: 2/24; visit 2: 2/24) and C5 (visit 1: 0/24; visit 2: 1/24). Over the contralateral hemisphere (Fig. 3A, right), the electrodes closest to the white matter fibres' terminations area were C4 (visit 1: 13/24; visit 2: 13/24), FC4 (visit 1: 1/24; visit 2: 2/24), C2 (visit 1: 7/24; visit 2: 4/24), CP4 (visit 1: 2/24; visit 2: 1/24), FC2 (visit 1: 1/24; visit 2: 2/24), C6 (visit 1: 0/24; visit 2: 1/24) and P4 (visit 1: 0/24; visit 2: 1/24). For further details on the electrodes employed for the analysis for each

subject and for each visit, see Supporting information, Table S1.

For the peak/trough ratio (Fig. 3B), we found a rate around 1 regardless of the temporal thresholds of sensitivity in the trial subdivision, meaning that the same number of peak and trough trials was found: unconstrained (visit 1: mean = 0.70, SEM = 0.10; visit 2: mean = 1.22, SEM = 0.30), 40 ms (visit 1: mean = 0.71, SEM = 0.10; visit 2: mean = 1.22, SEM = 0.30), 30 ms (visit 1: mean = 0.72, SEM = 0.11; visit 2: mean = 1.23, SEM = 0.32), 20 ms (visit 1: mean = 0.79, SEM = 0.17; visit 2: mean = 1.39, SEM = 0.43), 10 ms (visit 1: mean = 0.67, SEM = 0.12; visit 2: mean = 1.24,

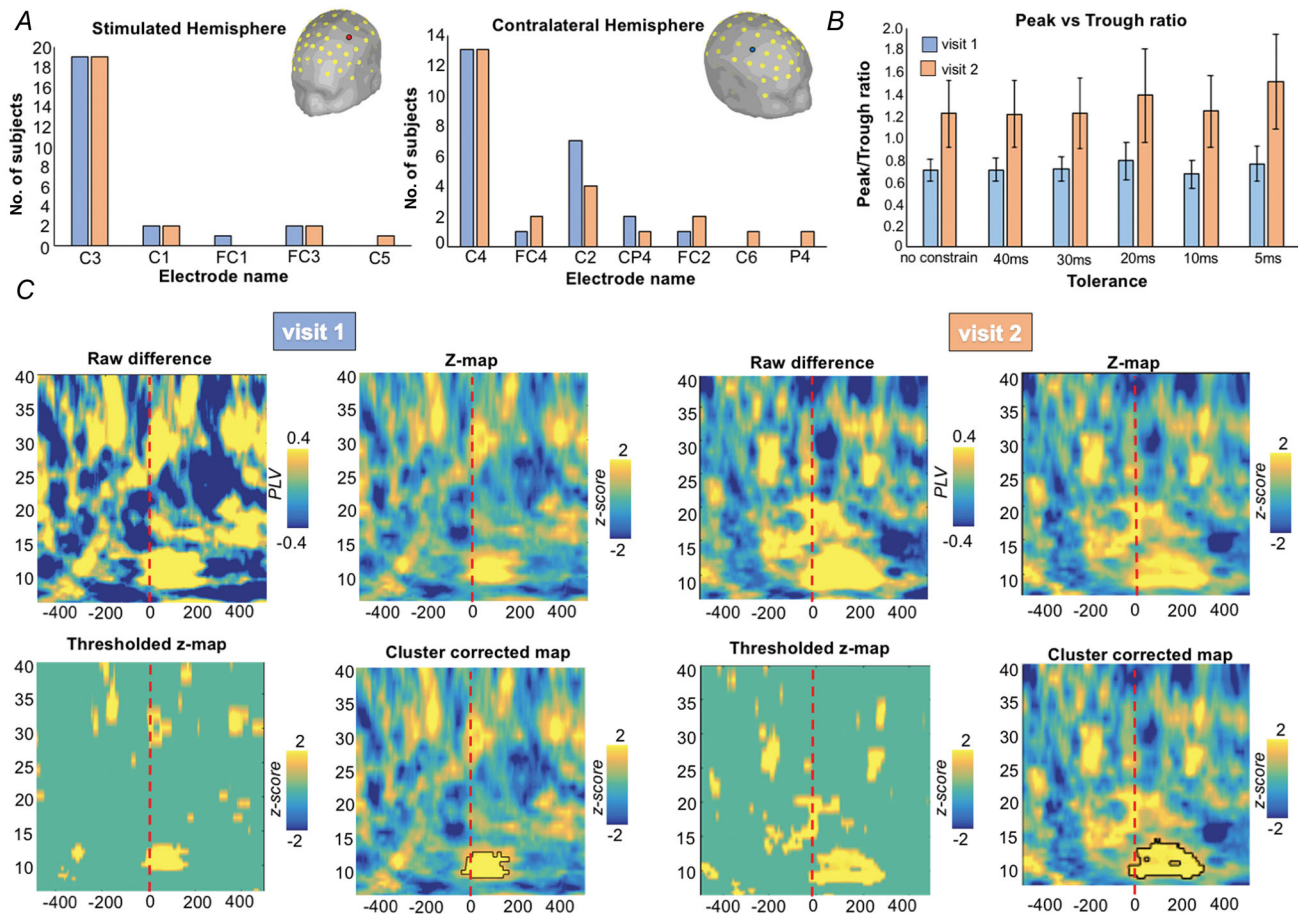


**Figure 3. Time–frequency PLV results comparing trough vs. peak for 5 ms thresholds of sensitivity**

A, in the majority of the subject and across visits, the electrode directly most affected by the TMS pulse was C3 ( $n$ : 19/24) for the stimulated hemisphere and C4 ( $n$ : 13/24) for the contralateral hemisphere. B, ratio of trials classified as peak or trough considering different degree of temporal sensitivity in the trial split selection (from no constraint to a minimum of a 5 ms window). C, the time–frequency PLV for the thresholds of sensitivity of 5 ms is shown. Raw difference plot represents the subtraction between trough vs. peak trials. Then the time–frequency matrices for peak and trough were transformed into z-values (z-map plot) and statistically compared to a null distribution of surrogate conditions obtained by swapping condition labels at each of 1000 permutations. The resulting z-scores were thresholded at  $P < 0.05$  (thresholded z-map). Finally, a distribution of cluster sizes of contiguous significant points under the null hypothesis of no condition difference was computed, and only the time–frequency clusters that exceeded the 95th percentile of this distribution were retained (cluster corrected-map). Trough trials were observed to induce greater synchronization between the selected electrode in the  $\mu$ -band compared to peak trials for both visit 1 and visit 2. [Colour figure can be viewed at [wileyonlinelibrary.com](http://wileyonlinelibrary.com)]

SEM = 0.33) and 5 ms (visit 1: mean = 0.76, SEM = 0.16; visit 2: mean = 1.52, SEM = 0.44).

### Electrode level phase-based connectivity between left and right hemisphere

As for 5 ms thresholds of sensitivity in splitting the trials (Fig. 3C), the time–frequency PLV showed a greater synchronization between the selected electrode after the TMS pulse in the  $\mu$ -band for the trough compared to peak trials for both visit 1 (average frequency = 11.35 Hz) and visit 2 (average frequency = 11.23 Hz).

Interestingly, such a result was independent of the thresholds of temporal sensitivity used to subdivide the trials (Fig. 4). Indeed, for both visits the same higher synchronization between the selected electrode in the  $\mu$ -band was evident for trough relative to peak trials: unconstrained (visit 1: average frequency = 12.97; visit 2: average frequency = 11.54), 40 ms (visit 1: average frequency = 12.84; visit 2: average frequency = 11.52), 30 ms (visit 1: average frequency = 12.72; visit 2: average frequency = 11.34), 20 ms (visit 1: average frequency = 12.59; visit 2: average frequency = 11.73), 10 ms (visit 1: average frequency = 12.44; visit 2: average frequency = 11.67) and 5 ms (visit 1: average frequency = 12.53; visit 2: average frequency = 12.02).

### Control analyses

As shown in Fig. 5A, EEG trial categorization was reliably performed both using resting-state and TMS–EEG

datasets. This demonstrates that even though it is known to be notoriously challenging to identify the phase properly in the presence of TMS-related (residual) artefacts and evoked responses (Zrenner *et al.* 2020), such TMS-induced contamination of the signal does not compromise the overall ability to categorize the trials accurately. For further details on the similarity between resting-state and TMS–EEG topoplots for both peak and trough, see Supporting information, Table S2.

As shown in Fig. 5B, a significant interaction Time  $\times$  Trial  $\times$  Frequency was found in the  $2 \times 2 \times 4$  ANOVA ( $F_{(2,42)} = 8.17$ ,  $P = 0.003$ ) with a significant interaction Time  $\times$  Frequency ( $F_{(1,21)} = 9.87$ ,  $P = 0.002$ ) and Time  $\times$  Trial ( $F_{(1,21)} = 11.45$ ,  $P < 0.001$ ). *Post hoc* level comparisons revealed that the pattern driven by trough trials with a significant difference was found in the theta (Post-TMS > Pre-TMS:  $t$ -value = 0.06,  $P = 0.002$ ) and alpha (post-TMS > pre-TMS:  $t$ -value = 2.14,  $P = 0.003$ ) frequency bands.

### Relationship between DWI metric and synchronization

To investigate the association between the significant trough vs. peak synchronization in the  $\mu$ -band and brain structure, separate non-parametric permutation GLM analyses with individual PLV as dependent variable and FD, FC, or FDC as independent variables were run. As shown in Fig. 6, a significant positive relationship was found between the amount of synchronization for both peak and trough trials and the FDC of the transcallosal

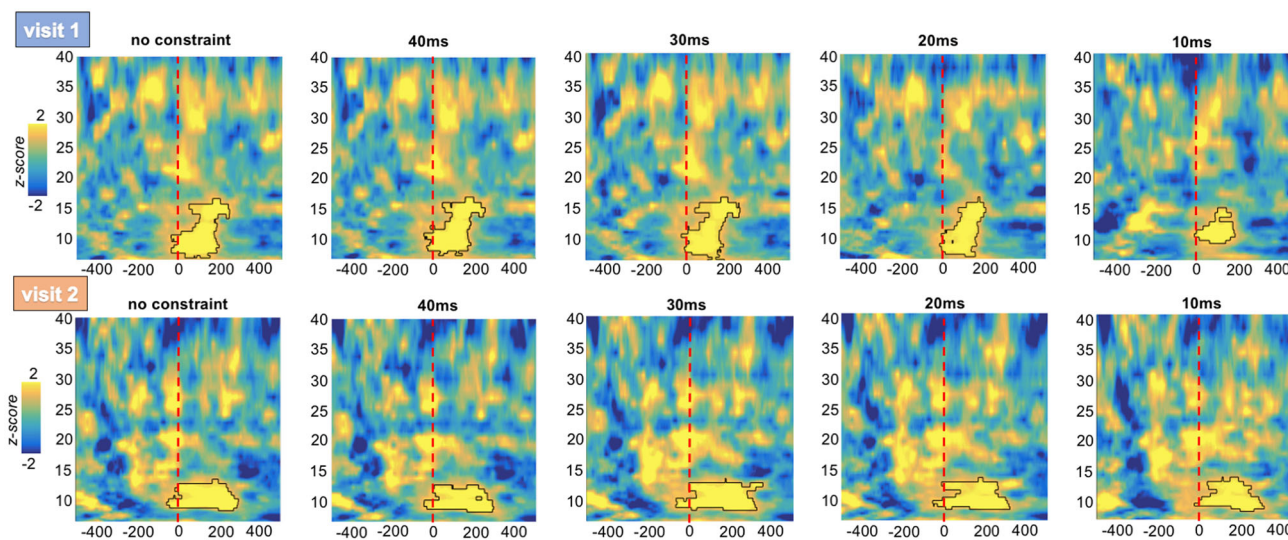


**Figure 4. Time–frequency PLV results comparing trough vs. peak for difference ms thresholds of sensitivity**

The time–frequency PLV for different thresholds of sensitivity in redistributing trough and peak trials is shown. For both visits, the same higher synchronization between the selected electrode in the  $\mu$ -band was evident for trough relative to peak trials. [Colour figure can be viewed at [wileyonlinelibrary.com](http://wileyonlinelibrary.com)]

corpus callosum fibres connecting the primary motor cortices ( $P < 0.05$ , FWE-corrected).

### Discussion

Previous studies have shown how TMS protocols synchronized with the phase of spontaneous brain oscillations result in long-term changes of excitability of the stimulated neural circuit, at both brain (Desideri

*et al.* 2019) and behavioural level (Zrenner *et al.* 2018). Here, we further expand this concept demonstrating how external perturbation of the motor network delivered at the negative peak of ongoing  $\mu$ -oscillations seems able to induce stronger c-c synchronization between the stimulated area and contralateral homologous regions belonging to the same network, with results being particularly relevant for the engagement and coupling of other non-motor networks of the brain.

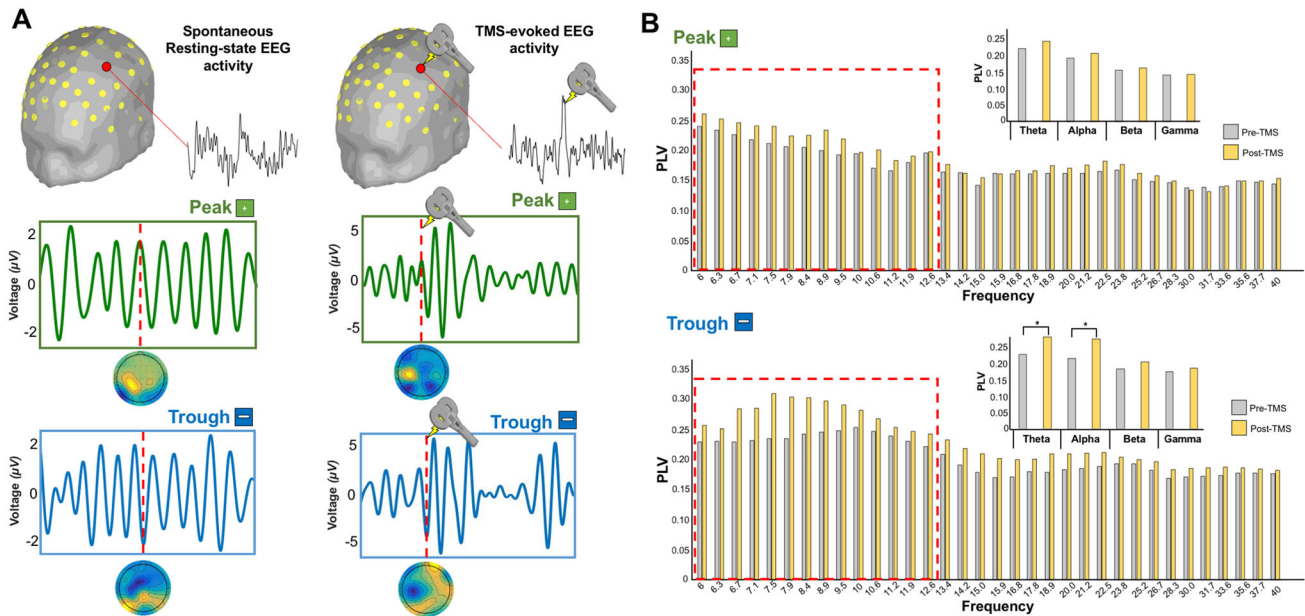


**Figure 5. Control analyses**  
 A, peak and trough trial categorization was performed using EEG data collected during resting-state eyes open. The resulting topomaps showed a comparable pattern to the TMS-EEG data demonstrating that TMS-related (residual) artefacts do not compromise the overall ability to categorize the trials accurately. B, grand mean average of PLV extracted for all the frequencies for both pre-TMS and post-TMS time window. A significant difference (red square boxes) was found in the theta (Post-TMS > Pre-TMS:  $t$ -value = 3.06,  $P = 0.002$ ) and alpha (post-TMS > pre-TMS:  $t$ -value = 2.14,  $P = 0.003$ ) frequency bands for trough compared to peak trials. [Colour figure can be viewed at wileyonlinelibrary.com]

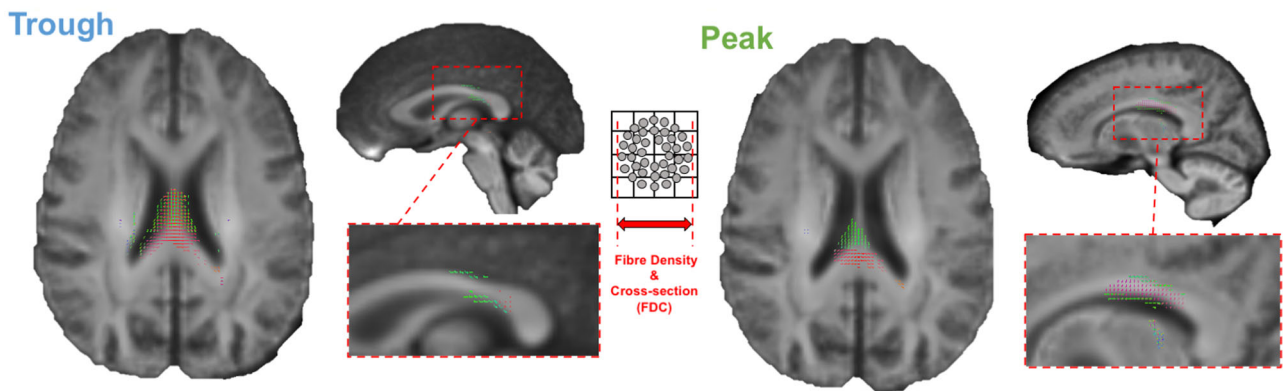


**Figure 6. Microstructural predictors of cortico-cortical synchronization**  
 A significant positive relationship was found between the amount of synchronization for both peak and trough trials, and the FDC of the transcallosal corpus callosum fibres connecting the primary motor cortices ( $P < 0.05$ , FWE-corrected). [Colour figure can be viewed at wileyonlinelibrary.com]

Finally, the microstructural nature of the stimulated white matter bundle was significantly related to the amount of synchronization, suggesting that axonal properties are relevant for the propagation of action potentials regardless of the phase moment when the external perturbation was delivered.

### TMS at trough induces higher cortico-cortical synchronization

In line with our hypothesis, external perturbations delivered at the negative peak of spontaneous  $\mu$ -oscillations induced higher c-c synchrony between the stimulated area and the contralateral homologous brain region of the same network, compared to the positive peak. Moreover, our control analyses revealed that such a result was specific for theta and alpha frequency bands and importantly was not driven by pre-TMS differences in the c-c synchronization values across the conditions. Previous single cell recordings on the rat have shown that stimulated pyramidal cells discharge mostly on the negative phase, corresponding to the time when the soma is least hyperpolarized (Buzsáki *et al.* 1983; Fox *et al.* 1986). In this framework, recent TMS-EEG studies in humans have shown how corticospinal excitability is enhanced at the negative compared to the positive peak of the  $\mu$ -oscillation as measured by MEP (Zrenner *et al.* 2018) and TEP (Desideri *et al.* 2019) amplitude. Indeed, following TMS-induced E-field modelling, external perturbation over motor hand area excites fibres in the pre- and postcentral gyrus parallel to the magnetic field (Laakso *et al.* 2014; Bungert *et al.* 2017). Such input leads to trans-synaptic activation of the apical dendritic trees of pyramidal cells (Amassian *et al.* 1987), which has been indicated as the main generator of negative deflections in the surface EEG (Buzsáki *et al.* 2012). For this reason, an external perturbation delivered at the negative peak of the  $\mu$ -rhythm reaches the dendritic trees of pyramidal cells at a time when they are closer to the firing threshold, leading to a higher fraction of them being recruited (Buzsáki *et al.* 1983; Kamondi *et al.* 1998). In this context, our retrospective analyses provide the first evidence that stimulation-induced connectivity changes within the targeted brain networks depend on the phase of the ongoing endogenous brain oscillations at the time of stimulation. In line with the aforementioned physiological studies, we have shown that the EEG negative peak of the  $\mu$ -oscillation represents the phase instant to induce higher c-c connectivity in homologous brain areas belonging to the same networks at source level, and not only a high-excitability state of corticospinal neurons as previously demonstrated (Zrenner *et al.* 2018). Importantly, the same result was obtained at electrode level where the spatial resolution is lower compared to source-based

reconstruction, even though we have tried to overcome this issue using a multimodal neuroimaging approach for the electrode selection. Such procedures overcome the fundamental limitations of individual modalities and should be potentially extended to other cognitive domains where the variability in the brain anatomy and geometry is higher.

Early experimental evidence in cats found that inter-hemispheric oscillatory synchronization between homologous neural assemblies in primary visual cortex is fundamental for establishing the relationship between distributed features in the two visual hemi-fields (Engel *et al.* 1991). Moreover, in the motor system, anatomical tracer work in non-human primates has demonstrated that the main callosal connections of the primary motor cortex (M1) are with homologous regions of the contralateral hemisphere (Rouiller *et al.* 1994; Dancause *et al.* 2007). From a functional perspective, whilst the  $\beta$ -frequency transiently synchronizes the two hemispheres during bimanual and unimanual motor tasks (Murthy & Fetz, 1996), the  $\mu$ -band constitutes the dominant rhythm in the frequency spectrum between homologous areas of the sensorimotor cortex at rest (Gastaut & Bert, 1954).

Overall, in line with the state-dependency effect of TMS (Silvanto & Pascual-Leone, 2008), our findings demonstrate that the effect of a given stimulus on the brain is highly dependent on the brain oscillation phase at that instant and not simply on the nature of the stimulus itself. Thus, given the high variability in outcome of the TMS application for the treatment of brain disorders, future studies should test whether stimuli synchronized with the individual patient's instantaneous brain state would improve the outcome of the intervention.

### Neural predictors of cortico-cortical synchronization

Apart from estimating the impact of a given intervention, identifying specific features predicting the likelihood of higher or lower responsiveness to a given treatment or therapy is becoming crucial in clinical and non-clinical settings (Drysdale *et al.* 2017). We highlighted a very interesting, yet preliminary, predictor of TMS-induced c-c synchronization in the FDC of the transcallosal fibres of the corpus callosum. Several studies have reported a positive relationship between microstructure of fibre tracts connecting bilateral primary motor cortices and the strength of interhemispheric inhibition, as measured in adults with short interval interhemispheric inhibition (Wahl *et al.* 2007; Fling *et al.* 2011). Furthermore, recent biophysical models of axon conduction have demonstrated a linear relationship between the delay of a simulated local field potential and the structural properties of transcallosal corpus callosum fibres (i.e. length and g-ratio) (Berman *et al.* 2019).

In this framework, our findings demonstrate that microstructural properties (both axonal density and bundle size) of the white matter tract connecting the two primary motor cortices was linearly related with the amount of synchronization. The fact that such a result was found for both peak and trough trials might suggest that an external perturbation would engage the same neuronal population and white matter fibres regardless of the phase period when the stimulus is delivered. Conversely, it is the amount of information conveyed by the white matter tract that is highly dependent on the phase moment when the TMS pulse is applied. Prospective studies including a predefined assignment to a low and high corpus callosum fibre FDC group are needed to causally validate this hypothesis.

### Limitations of the study and future directions

Our results must be interpreted considering the low spatial resolution of the EEG. Despite our selecting the electrode based on individual white matter tracts obtained by a high spatial resolution DWI acquisition, a more precise spatial mapping of TMS-induced network effects would be better captured by ideally combining TMS–EEG with concurrent fMRI acquisitions (Peters *et al.* 2020).

As for the time–frequency EEG analysis, one important limitation concerns the fact that we have not tested potential changes in *c-c* connectivity of other frequency band oscillations. However, selecting the  $\mu$ -rhythm was well grounded on previous research (Hari, 2006; Jensen & Mazaheri, 2010; Haegens *et al.* 2011; Stefanou *et al.* 2020), while results on other oscillation bands have been demonstrated to be contradictory (Guerra *et al.* 2016; Raco *et al.* 2016). Moreover, in addition to being previously reported, using the  $\mu$ -rhythm made the classification of the trial for negative and positive peaks easier than when using other bands with higher frequency.

It is important to mention that the statistical analysis at the electrode level was performed treating the two visits as independent. Indeed, the main goal of the study was to investigate differences between the condition (peak and trough) across the two visits. For this reason, a condition-wise (instead of visit-wise) permutation testing was performed in order to control for type I error (Maris & Oostenveld, 2007). Furthermore, cluster-based thresholding (Pernet *et al.* 2015) was performed, retaining only clusters that exceeded the 95th percentile of the distributions of contiguous significant points obtained for all the permutations.

Furthermore, as for the diffusion signal, future studies might employ quantitative MRI techniques combined with advanced biophysical models to measure microstructural features of white matter, such as axon diameter, the *g*-ratio and the overall tract length (Duval *et al.* 2017).

In addition, future studies should integrate diffusion and functional MRI to constrain the resolution of the EEG inverse problem in order to evaluate the transfer of information through the white matter on a millisecond scale (Deslauriers-Gauthier *et al.* 2019).

Finally, future studies should explore whether such a phase-dependent effect of TMS can be extended to other resting state networks involved in high cognitive functioning.

### Conclusion

Our analyses expand on previous studies by demonstrating how TMS pulses delivered at a specific phase instant result in differential long-distance connectivity values within the stimulated network, depending on the phase of the targeted oscillation. Moreover, such *c-c* synchronization changes are linearly predicted by the microstructure of the white matter tract that connects the two brain regions, regardless of the phase state when the stimulus was delivered. Findings can be used to tailor – or predict the impact of – interventions targeting other sensory as well as cognitive brain networks outside the motor system, such as the default mode or dorsal attention networks.

### References

- Akam T & Kullmann DM (2014). Oscillatory multiplexing of population codes for selective communication in the mammalian brain. *Nat Rev Neurosci* **15**, 111–122.
- Amassian VE, Stewart M, Quirk GJ & Rosenthal JL (1987). Physiological basis of motor effects of a transient stimulus to cerebral cortex. *Neurosurgery* **20**, 74–93.
- Andersson JLR & Sotiropoulos SN (2016). An integrated approach to correction for off-resonance effects and subject movement in diffusion MR imaging. *Neuroimage* **125**, 1063–1078.
- Avants BB, Tustison NJ, Song G, Cook PA, Klein A & Gee JC (2011). A reproducible evaluation of ANTs similarity metric performance in brain image registration. *Neuroimage* **54**, 2033–2044.
- Bergmann TO, Lieb A, Zrenner C & Ziemann U (2019). Pulsed facilitation of corticospinal excitability by the sensorimotor  $\mu$ -alpha rhythm. *J Neurosci* **39**, 10034–10043.
- Berman S, Filo S & Mezer AA (2019). Modeling conduction delays in the corpus callosum using MRI-measured *g*-ratio. *Neuroimage* **195**, 128–139.
- Bortoletto M, Bonzano L, Zazio A, Ferrari C, Pedullà L, Gasparotti R, Miniussi C & Bove M (2021). Asymmetric transcallosal conduction delay leads to finer bimanual coordination. *Brain Stimul* **14**, 379–388.
- Bungert A, Antunes A, Espenhahn S & Thielscher A (2017). Where does TMS stimulate the motor cortex? Combining electrophysiological measurements and realistic field estimates to reveal the affected cortex position. *Cereb Cortex* **27**, 5083–5094.

- Buzsáki G (2006). *Rhythms of the Brain*. Oxford University Press, Oxford.
- Buzsáki G, Anastassiou CA & Koch C (2012). The origin of extracellular fields and currents – EEG, ECoG, LFP and spikes. *Nat Rev Neurosci* **13**, 407–420.
- Buzsáki G & Draguhn A (2004). Neuronal oscillations in cortical networks. *Science* **304**, 1926–1929.
- Buzsáki G, Lai-Wo SL & Vanderwolf CH (1983). Cellular bases of hippocampal EEG in the behaving rat. *Brain Res Rev* **6**, 139–171.
- Cohen MX (2017). Rigor and replication in time-frequency analyses of cognitive electrophysiology data. *Int J Psychophysiol* **111**, 80–87.
- Connolly KR, Helmer A, Cristancho MA, Cristancho P & O'Reardon JP (2012). Effectiveness of transcranial magnetic stimulation in clinical practice post-FDA approval in the United States: results observed with the first 100 consecutive cases of depression at an academic medical center. *J Clin Psychiatry* **73**, e567–e573.
- Corcoran AW, Alday PM, Schlesewsky M & Bornkessel-Schlesewsky I (2018). Toward a reliable, automated method of individual alpha frequency (IAF) quantification. *Psychophysiology* **55**, e13064.
- Dancause N, Barbay S, Frost SB, Mahnken JD & Nudo RJ (2007). Interhemispheric connections of the ventral pre-motor cortex in a new world primate. *J Comp Neurol* **505**, 701–715.
- Delorme A & Makeig S (2004). EEGLAB: an open source toolbox for analysis of single-trial EEG dynamics including independent component analysis. *J Neurosci Methods* **134**, 9–21.
- Desideri D, Zrenner C, Ziemann U & Belardinelli P (2019). Phase of sensorimotor  $\mu$ -oscillation modulates cortical responses to transcranial magnetic stimulation of the human motor cortex. *J Physiol* **597**, 5671–5686.
- Deslauriers-Gauthier S, Lina J-M, Butler R, Whittingstall K, Gilbert G, Bernier P-M, Deriche R & Descoteaux M (2019). White matter information flow mapping from diffusion MRI and EEG. *Neuroimage* **201**, 116017.
- Dhollander T & Connelly A (2016). A novel iterative approach to reap the benefits of multi-tissue CSD from just single-shell ( $+b = 0$ ) diffusion MRI data. *Proc Intl Soc Mag Reson Med* **24**, 3010.
- Drysdale AT, Grosenick L, Downar J, Dunlop K, Mansouri F, Meng Y, Fetcho RN, Zebly B, Oathes DJ, Etkin A, Schatzberg AF, Sudheimer K, Keller J, Mayberg HS, Gunning FM, Alexopoulos GS, Fox MD, Pascual-Leone A, Voss HU, Casey BJ, Dubin MJ & Liston C (2017). Resting-state connectivity biomarkers define neurophysiological subtypes of depression. *Nat Med* **23**, 28–38.
- Duval T, Stikov N & Cohen-Adad J (2017). Modeling white matter microstructure. *Funct Neurol* **31**, 217–228.
- Engel AK, Kreiter AK, Konig P & Singer W (1991). Synchronization of oscillatory neuronal responses between striate and extrastriate visual cortical areas of the cat. *Proc Natl Acad Sci U S A* **88**, 6048–6052.
- Fischl B, van der Kouwe A, Destrieux C, Halgren E, Ségonne F, Salat DH, Busa E, Seidman LJ, Goldstein J, Kennedy D, Caviness V, Makris N, Rosen B & Dale AM (2004). Automatically parcellating the human cerebral cortex. *Cereb Cortex* **14**, 11–22.
- Fling BW, Benson BL & Seidler RD (2011). Transcallosal sensorimotor fibre tract structure-function relationships. *Hum Brain Mapp* **34**, 384–395.
- Fox SE, Wolfson S & Ranck JB (1986). Hippocampal theta rhythm and the firing of neurons in walking and urethane anesthetized rats. *Exp Brain Res* **62**, 495–508.
- Gastaut HJ & Bert J (1954). EEG changes during cinematographic presentation (moving picture activation of the EEG). *Electroencephalogr Clin Neurophysiol* **6**, 433–444.
- Gramfort A, Luessi M, Larson E, Engemann DA, Strohmeier D, Brodbeck C, Goj R, Jas M, Brooks T, Parkkonen L & Hämäläinen M (2013). MEG and EEG data analysis with MNE-Python. *Front Neurosci* **7**, 267.
- Gramfort A, Papadopoulos T, Olivi E & Clerc M (2010). OpenMEEG: opensource software for quasistatic bioelectromagnetics. *Biomed Eng OnLine* **9**, 45.
- Guerra A, Pogosyan A, Nowak M, Tan H, Ferreri F, Di Lazzaro V & Brown P (2016). Phase dependency of the human primary motor cortex and cholinergic inhibition cancellation during beta tACS. *Cereb Cortex* **26**, 3977–3990.
- Haegens S, Nächer V, Luna R, Romo R & Jensen O (2011).  $\alpha$ -Oscillations in the monkey sensorimotor network influence discrimination performance by rhythmical inhibition of neuronal spiking. *Proc Natl Acad Sci U S A* **108**, 19377–19382.
- Hämäläinen MS & Ilmoniemi RJ (1994). Interpreting magnetic fields of the brain: minimum norm estimates. *Med Biol Eng Comput* **32**, 35–42.
- Hari R (2006). Action-perception connection and the cortical mu rhythm. *Prog Brain Res* **159**, 253–260.
- Hussain SJ, Hayward W, Fourcand F, Zrenner C, Ziemann U, Buch ER, Hayward MK & Cohen LG (2020). Phase-dependent transcranial magnetic stimulation of the lesioned hemisphere is accurate after stroke. *Brain Stimulat* **13**, 1354–1357.
- Hyvärinen A & Oja E (1997). A fast fixed-point algorithm for independent component analysis. *Neural Comput* **9**, 1483–1492.
- Jenkinson M, Beckmann CF, Behrens TEJ, Woolrich MW & Smith SM (2012). FSL. *Neuroimage* **62**, 782–790.
- Jensen O & Mazaheri A (2010). Shaping functional architecture by oscillatory alpha activity: gating by inhibition. *Front Hum Neurosci* **4**, 186.
- Kamondi A, Acsády L, Wang XJ & Buzsáki G (1998). Theta oscillations in somata and dendrites of hippocampal pyramidal cells in vivo: activity-dependent phase-precession of action potentials. *Hippocampus* **8**, 244–261.
- Laakso I, Hirata A & Ugawa Y (2014). Effects of coil orientation on the electric field induced by TMS over the hand motor area. *Phys Med Biol* **59**, 203–218.
- Lachaux J-P, Rodriguez E, Martinerie J & Varela FJ (1999). Measuring phase synchrony in brain signals. *Hum Brain Mapp* **8**, 194–208.

- López-Alonso V, Cheeran B, Río-Rodríguez D & Fernández-del-Olmo M (2014). Inter-individual variability in response to non-invasive brain stimulation paradigms. *Brain Stimul Basic Transl Clin Res Neuromodul* **7**, 372–380.
- Madsen KH, Karabanov AN, Krohne LG, Safeldt MG, Tomasevic L & Siebner HR (2019). No trace of phase: corticomotor excitability is not tuned by phase of pericentral  $\mu$ -rhythm. *Brain Stimulat* **12**, 1261–1270.
- Maris E & Oostenveld R (2007). Nonparametric statistical testing of EEG- and MEG-data. *J Neurosci Methods* **164**, 177–190.
- Momi D, Ozdemir RA, Tadayon E, Boucher P, Shafi MM, Pascual-Leone A & Santarnecchi E (2020). Network-level macroscale structural connectivity predicts propagation of transcranial magnetic stimulation. *Neuroimage* **229**, 117698.
- Mormann F, Lehnertz K, David P & Elger CE (2000). Mean phase coherence as a measure for phase synchronization and its application to the EEG of epilepsy patients. *Phys D* **144**, 358–369.
- Murthy VN & Fetz EE (1996). Oscillatory activity in sensorimotor cortex of awake monkeys: synchronization of local field potentials and relation to behavior. *J Neurophysiol* **76**, 3949–3967.
- Oldfield RC (1971). The assessment and analysis of handedness: the Edinburgh inventory. *Neuropsychologia* **9**, 97–113.
- Perera T, George MS, Grammer G, Janicak PG, Pascual-Leone A & Wirecki TS (2016). The clinical TMS society consensus review and treatment recommendations for TMS therapy for major depressive disorder. *Brain Stimulat* **9**, 336–346.
- Pernet CR, Latinus M, Nichols TE & Rousselet GA (2015). Cluster-based computational methods for mass univariate analyses of event-related brain potentials/fields: a simulation study. *J Neurosci Methods* **250**, 85–93.
- Peters JC, Reithler J, de Graaf TA, Schuhmann T, Goebel R & Sack AT (2020). Concurrent human TMS-EEG-fMRI enables monitoring of oscillatory brain state-dependent gating of cortico-subcortical network activity. *Commun Biol* **3**, 40.
- Raco V, Bauer R, Tharsan S & Gharabaghi A (2016). Combining TMS and tACS for closed-loop phase-dependent modulation of corticospinal excitability: a feasibility study. *Front Cell Neurosci* **10**, 143.
- Raffelt D, Tournier J-D, Rose S, Ridgway GR, Henderson R, Crozier S, Salvado O & Connelly A (2012). Apparent fibre density: a novel measure for the analysis of diffusion-weighted magnetic resonance images. *Neuroimage* **59**, 3976–3994.
- Raffelt DA, Tournier J-D, Smith RE, Vaughan DN, Jackson G, Ridgway GR & Connelly A (2017). Investigating white matter fibre density and morphology using fixel-based analysis. *Neuroimage* **144**, 58–73.
- Rogasch NC, Sullivan C, Thomson RH, Rose NS, Bailey NW, Fitzgerald PB, Farzan F & Hernandez-Pavon JC (2017). Analysing concurrent transcranial magnetic stimulation and electroencephalographic data: a review and introduction to the open-source TESA software. *Neuroimage* **147**, 934–951.
- Romero MC, Davare M, Armendariz M & Janssen P (2019). Neural effects of transcranial magnetic stimulation at the single-cell level. *Nat Commun* **10**, 2642.
- Rossi S, Antal A, Bestmann S, Bikson M, Brewer C, Brockmüller J, Carpenter LL, Cincotta M, Chen R, Daskalakis JD, Di Lazzaro V, Fox MD, George MS, Gilbert D, Kimiskidis VK, Koch G, Ilmoniemi RJ, Lefaucheur JP, Leocani L, Lisanby SH, Miniussi C, Padberg F, Pascual-Leone A, Paulus W, Peterchev AV, Quartarone A, Rotenberg A, Rothwell J, Rossini PM, Santarnecchi E, Shafi MM, Siebner HR, Ugawa Y, Wassermann EM, Zangen A, Ziemann U & Hallett M (2020). Safety and recommendations for TMS use in healthy subjects and patient populations, with updates on training, ethical and regulatory issues: expert guidelines. *Clin Neurophysiol* **132**, 269–306.
- Rossini PM, Burke D, Chen R, Cohen LG, Daskalakis Z, Di Iorio R, Di Lazzaro V, Ferreri F, Fitzgerald PB, George MS, Hallett M, Lefaucheur JP, Langguth B, Matsumoto H, Miniussi C, Nitsche MA, Pascual-Leone A, Paulus W, Rossi S, Rothwell JC, Siebner HR, Ugawa Y, Walsh V & Ziemann U (2015). Non-invasive electrical and magnetic stimulation of the brain, spinal cord, roots and peripheral nerves: basic principles and procedures for routine clinical and research application. An updated report from an I.F.C.N. committee. *Clin Neurophysiol* **126**, 1071–1107.
- Rothwell JC, Hallett M, Berardelli A, Eisen A, Rossini P & Paulus W (1999). Magnetic stimulation: motor evoked potentials. The international federation of clinical neurophysiology. *Electroencephalogr Clin Neurophysiol Suppl* **52**, 97–103.
- Rouiller EM, Babalian A, Kazennikov O, Moret V, Yu XH & Wiesendanger M (1994). Transcallosal connections of the distal forelimb representations of the primary and supplementary motor cortical areas in macaque monkeys. *Exp Brain Res* **102**, 227–243.
- Schaefer A, Kong R, Gordon EM, Laumann TO, Zuo X-N, Holmes AJ, Eickhoff SB & Yeo BTT (2018). Local-global parcellation of the human cerebral cortex from intrinsic functional connectivity MRI. *Cereb Cortex* **28**, 3095–3114.
- Schaworonkow N, Triesch J, Ziemann U & Zrenner C (2019). EEG-triggered TMS reveals stronger brain state-dependent modulation of motor evoked potentials at weaker stimulation intensities. *Brain Stimulat* **12**, 110–118.
- Silvanto J & Pascual-Leone A (2008). State-dependency of transcranial magnetic stimulation. *Brain Topogr* **21**, 1–10.
- Smith RE, Tournier J-D, Calamante F & Connelly A (2012). Anatomically-constrained tractography: improved diffusion MRI streamlines tractography through effective use of anatomical information. *Neuroimage* **62**, 1924–1938.
- Stefanou M-I, Desideri D, Belardinelli P, Zrenner C & Ziemann U (2018). Phase synchronicity of  $\mu$ -rhythm determines efficacy of interhemispheric communication between human motor cortices. *J Neurosci* **38**, 10525–10534.
- Stefanou M-I, Galevska D, Zrenner C, Ziemann U & Nieminen JO (2020). Interhemispheric symmetry of  $\mu$ -rhythm phase-dependency of corticospinal excitability. *Sci Rep* **10**, 7853.

- Tenke CE & Kayser J (2012). Generator localization by current source density (CSD): implications of volume conduction and field closure at intracranial and scalp resolutions. *Clin Neurophysiol* **123**, 2328–2345.
- ter Braack EM, de Vos CC & van Putten MJAM (2015). Masking the auditory evoked potential in TMS-EEG: a comparison of various methods. *Brain Topogr* **28**, 520–528.
- Thielscher A, Antunes A & Saturnino GB (2015). Field modeling for transcranial magnetic stimulation: a useful tool to understand the physiological effects of TMS? *Annu Int Conf IEEE Eng Med Biol Soc* **2015**, 222–225.
- Thut G & Pascual-Leone A (2010). Integrating TMS with EEG: how and what for? *Brain Topogr* **22**, 215–218.
- Tournier J-D, Calamante F & Connelly A (2007). Robust determination of the fibre orientation distribution in diffusion MRI: non-negativity constrained super-resolved spherical deconvolution. *Neuroimage* **35**, 1459–1472.
- Tournier J-D, Calamante F & Connelly A (2012). MRtrix: diffusion tractography in crossing fibre regions. *Int J Imaging Syst Technol* **22**, 53–66.
- Uhlhaas PJ & Singer W (2010). Abnormal neural oscillations and synchrony in schizophrenia. *Nat Rev Neurosci* **11**, 100–113.
- Veraart J, Novikov DS, Christiaens D, Ades-Aron B, Sijbers J & Fieremans E (2016). Denoising of diffusion MRI using random matrix theory. *Neuroimage* **142**, 394–406.
- Voineskos AN, Farzan F, Barr MS, Lobaugh NJ, Mulsant BH, Chen R, Fitzgerald PB & Daskalakis ZJ (2010). The role of the corpus callosum in transcranial magnetic stimulation induced interhemispheric signal propagation. *Biol Psychiatry* **68**, 825–831.
- Wahl M, Lauterbach-Soon B, Hattingen E, Jung P, Singer O, Volz S, Klein JC, Steinmetz H & Ziemann U (2007). Human motor corpus callosum: topography, somatotopy, and link between microstructure and function. *J Neurosci* **27**, 12132–12138.
- Yeo BTT, Krienen FM, Sepulcre J, Sabuncu MR, Lashkari D, Hollinshead M, Roffman JL, Smoller JW, Zöllei L, Polimeni JR, Fischl B, Liu H & Buckner RL (2011). The organization of the human cerebral cortex estimated by intrinsic functional connectivity. *J Neurophysiol* **106**, 1125–1165.
- Zazio A, Miniussi C & Bortoletto M (2021). Alpha-band cortico-cortical phase synchronization is associated with effective connectivity in the motor network. *Clin Neurophysiol* **132**, 2473–2480.
- Zhang Y, Brady M & Smith S (2001). Segmentation of brain MR images through a hidden Markov random field model and the expectation-maximization algorithm. *IEEE Trans Med Imaging* **20**, 45–57.
- Zrenner C, Desideri D, Belardinelli P & Ziemann U (2018). Real-time EEG-defined excitability states determine efficacy of TMS-induced plasticity in human motor cortex. *Brain Stimulat* **11**, 374–389.
- Zrenner C, Galevska D, Nieminen JO, Baur D, Stefanou M-I & Ziemann U (2020). The shaky ground truth of real-time phase estimation. *Neuroimage* **214**, 116761.

## Additional Information

### Data availability statement

Data cannot be shared as participants were informed that their data would be stored confidentially, in accordance with the rules of the local ethics committee. Code for generating the E-field modeling maps, the DWI and the EEG metrics is available in <http://www.tmslab.org/netconlab-macroscale.php>

### Competing interests

A.P.-L. is a co-founder of Linus Health and TI Solutions AG; serves on the scientific advisory boards for Starlab Neuroscience, Neuroelectrics, Magstim Inc., Nexstim, Cognito and MedRhythms; and is listed as an inventor on several issued and pending patents on the real-time integration of non-invasive brain stimulation with electroencephalography and magnetic resonance imaging. E.S. serves on the scientific advisory boards of Neurocare, EBneuro; and is listed as an inventor on several issued and pending patents on the application of brain stimulation in patients with Alzheimer's disease and brain tumours. The authors declare no competing financial interests.

### Author contributions

D.M.: designed the study, conceptualization, conceptualized the framework, data curation, collected the data, preprocessed the TMS-EEG data, formal analysis, writing – original draft, pre-processed and analysed TMS-EEG data and wrote the first draft. R.A.O.: data curation, collected the data. E.T.: formal analysis and define individual TMS targets. P.B.: data curation, collected the data, preprocessed the TMS-EEG data. A.DiD.: writing – review and editing. M.F.: writing – review and editing. A.P.-L.: designed the study, writing – review and editing, oversaw study conduction and edited the first draft. M.M.S.: designed the study, conceptualization, conceptualized the framework, over-viewed the selection of stimulation sites, writing – review and editing, oversaw study conduction and edited the first draft. E.S.: designed the study, conceptualization, conceptualized the framework, overviewed the selection of stimulation sites, design data analysis, writing – review and editing, oversaw study conduction and edited the first draft, finalized final version of the manuscript. All authors have read and approved the final version of this manuscript and agree to be accountable for all aspects of the work in ensuring that questions related to the accuracy or integrity of any part of the work are appropriately investigated and resolved. All persons designated as authors qualify for authorship, and all those who qualify for authorship are listed.

### Funding

This work was supported by MIT-Harvard Broad institute Grant in Aid (6600024-5500000895), DARPA Grant (HR001117S0030), ADDF Grant (GA201902-2017902),



National Institutes of Health Grant (R01AG059089), and was supported by the National Science Foundation, and La Caixa.

### Acknowledgements

We are grateful for the gracious funding from the MIT-Harvard Broad institute (6600024-5500000895) directly supporting the study and our line of research on brain plasticity biomarkers. The authors would like to thank all participants who took part in the study and for their efforts. E.S. is supported by the Defence Advanced Research Projects Agency (DARPA) via HR001117S0030, the NIH (P01 AG031720-06A1, R01 MH117063-01, R01 AG060981-01), and ADDF (ADDF-FTD GA201902–2017902). M.M.S is supported by the Football Players Health Study (FPHS) at Harvard University, and the NIH (R01 MH115949, R01AG060987, P01 AG031720-06A1). A.P.-L. is supported by grants from the National Institutes of Health (P01 AG031720; R24AG06142; R01AG059089), National Science Foundation, and La Caixa. The content of this

paper is solely the responsibility of the authors and does not necessarily represent the official views of Harvard University and its affiliated academic health care centres or the National Institutes of Health.

### Keywords

brain-state dependent effect, cortico-cortical connectivity,  $\mu$ -rhythm, structural connectivity, TMS-EEG

### Supporting information

Additional supporting information can be found online in the Supporting Information section at the end of the HTML view of the article. Supporting information files available:

#### Peer Review History

#### Statistical Summary Document

#### Supplementary information